Available online at www.sciencedirect.com
ScienceDirect
Journal of the European Ceramic Society 27 (2007) 3977–3982
www.elsevier.com/locate/jeurceramsoc

Injection and selfconsistent charge transport in bulk insulators

H.-J. Fitting [a,*], N. Cornet [b], M. Touzin [b,c], D. Goeuriot [b], C. Guerret-Piécourt [c], D. Tréheux [c]

[a] *Physics Department, University of Rostock, Universitätsplatz 3, D-18051 Rostock, Germany*
[b] *Centre Sciences des Matériaux et des Structures, Ecole Nationale Supérieure des Mines de St. Etienne, 158 cours Fauriel, F-42023 Saint-Etienne cedex 2, France*
[c] *Laboratoire de Tribologie et Dynamique des Systémes, Ecole Centrale de Lyon, UMR CNRS 5513, 36 avenue Guy de Collongue, F-69134 Ecully cedex, France*

Available online 21 March 2007

Abstract

The new flight-drift model (FDM) of selfconsistent electron transport and electrical charge storage in wide-gap insulators reflects a more realistic simulation of these processes in dielectric and insulating materials than the former mainly ballistic model. Thus, electron-hole creation, their ballistic flight, followed by field-drift transport, and finally trapping in localized states and/or recombination are taken into account. The experimentally accessable quantities of field assisted secondary electron emission σ as well as the resulting surface potential V_0 due to internal current $j(x, t)$, charge $\rho(x, t)$, field $F(x, t)$, and potential $V(x, t)$ distributions are obtained. The calculations are performed for bulk Al_2O_3 ceramics with open and metal-coated and grounded surfaces.

Keywords: Insulators; Al_2O_3; Electrical conductivity; Dielectric properties

1. Introduction

Insulating and dielectric materials, especially as oxides, perovskites, ceramics, and functional layers become more and more important in modern technology.[1] Especially, the influence of dielectric polarization and charging on the features of these materials has been investigated more intensively and reported, e.g. on the conference series on Electric Charges in Non-Conductive Materials.[2,3] Furthermore, the electrical charging of insulators under different types of ionizing irradiation (electrons, neutrons, and X- γ-Rays) is of considerable interest in many fields of technology and science from the development of thermonuclear fusion (ITER) as a possible future source of energy, see ref.[4] to the multiform development of insulating materials for satellites and spacecrafts protection.[5] All these applications come within the same physical mechanism. Irradiation induces the injection of high energetic charges and generates electron-holes pairs. Secondary electrons are emitted but an important part of the charge carriers remains in the sample and its drift depends on the trapping properties of the material. The knowledge of these charging phenomena would help in preventing insulator breakdown mainly responsible for the damage of electronic devices.[6]

A first approach of these phenomena is based on the dynamic double layer model (DDLM) in which the phenomenon is brought to the simplified case of two layers of opposite charge. A solution of the respective equations were achieved by Melchinger and Hofmann.[7] More recently, Cazaux[8] developed a description of the SEE evolution in insulating samples using this DDLM.

The first comprehensive Monte Carlo calculations of the selfconsistent charging were made by Vicario et al.[9] Ganachaud et al.[10] and Renoud et al.[11,12] Of course, these calculations are complex because of the deal with the full simulation of primary electron straggling as well as with the generation and transport of secondary electrons and holes in the selfconsistent field. Nevertheless, it is of importance to enlighten this phenomenon of selfconsistent charging. One of the first attempts was the planar selfconsistent charging simulation of our co-author (HJF) already in 1978,[13,14] later on improved for insulating layers on conducting substrate in ref.[15] and for bulk materials in ref.[16] These authors use field-dependent attenuation lengths $\lambda(F)$ for the ballistic transport of electrons and holes which had been

* Corresponding author. Tel.: +49 381 4986760; fax: +49 381 4986802.

0955-2219/$ – see front matter © 2007 Elsevier Ltd. All rights reserved.
doi:10.1016/j.jeurceramsoc.2007.02.078

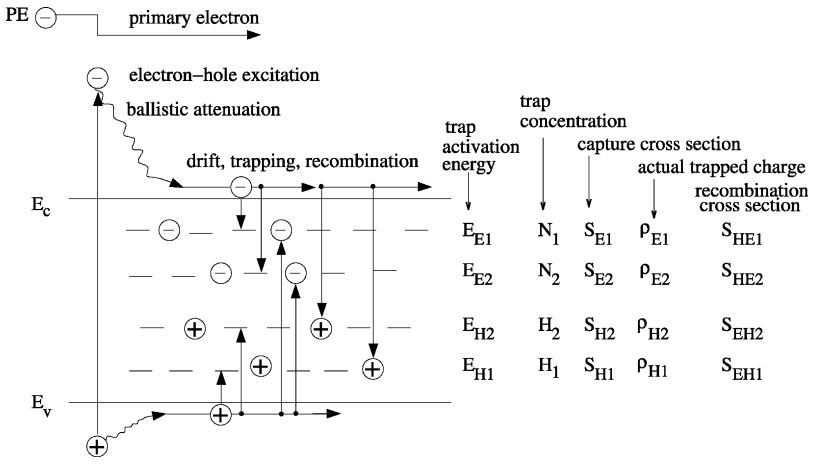

Fig. 1. Scheme of the flight-drift model including the ballistic flight and attenuation followed by drift, trapping, and recombination of electrons and holes in and/or via respective traps.

found experimentally by means of electron beam induced currents (EBIC) measurements[17,18] and had been verified by Monte Carlo calculations.[19,20,21,22]

The present paper will extend the ballistic flight model for electrons and holes to a more comprehensive and realistic new flight-drift model (FDM). There the ballistic flight of excited electrons and holes is followed by their drift and respective recombination and/or trapping in shallow and deep traps, see Fig. 1.

2. Electron and hole transport

The scattering and straggling of primary electrons (PE), their excitation of secondary electrons (SE) and holes (H) as well as the ballistic flight and attenuation of the latter ones as ballistic electrons (BE) and holes (BH), as presented schematically in Fig. 1, has been described partially in ref.[16] and more comprehensively in our recent paper.[23] In the present paper, we will pay attention to the new extensions, i.e. the drift of electrons and holes in selfconsistent fields, their recombination and/or trapping in localized states, i.e. traps, as well as their release from these traps by means of the Poole–Frenkel effect.[24,25]

These processes are included in the following Eq. (1) for drifting (D) electrons (E) in reverse (R) towards the surface and transmission (T) into bulk directions:

$$j_{\mathrm{DET}}^{\mathrm{DER}}(x) = \left\{ j_{\mathrm{DET}}^{\mathrm{DER}}(x \pm \Delta x) + \underbrace{\left[j_{\mathrm{BER}}(x)[1 - W_{\mathrm{EFR}}(x)] + j_{\mathrm{BET}}(x)[1 - W_{\mathrm{EFT}}(x)] \right]}_{\text{generation}} + \underbrace{\varrho_{\mathrm{E1}}(x) W_{\mathrm{E1PF}} + \varrho_{\mathrm{E2}}(x) W_{\mathrm{E2PF}}}_{\text{detrapping}} \right\} F_{\mathrm{E}}(x)$$
$$\times \underbrace{\exp\left[-\frac{\varrho_{\mathrm{H1}}}{e_0} S_{\mathrm{EH1}} \Delta x \right]}_{W_{\mathrm{EH1}}} \underbrace{\exp\left[-\frac{\varrho_{\mathrm{H2}}}{e_0} S_{\mathrm{EH2}} \Delta x \right]}_{W_{\mathrm{EH2}}} \underbrace{\exp\left[-\left(N_1 \frac{\varrho_{\mathrm{E1}}}{e_0} \right) S_{\mathrm{E1}} \Delta x \right]}_{W_{\mathrm{E1}}} \underbrace{\exp\left[-\left(N_2 - \frac{\varrho_{\mathrm{E2}}}{e_0} \right) S_{\mathrm{E2}} \Delta x \right]}_{W_{\mathrm{E2}}} \quad (1)$$

recombination; trapping

Here the convection term describes incoming and outgoing drifting electrons in the depth element Δx; the generation term presents the sources of drift electrons by attenuated (exhausted) ballistic electrons; the detrapping term is the Poole–Frenkel release of electrons from traps, presenting also a source of drifting electrons; the field factor F_{E} means the anisotropy of generated drifting electrons in the electric field F; and as electron drains we see the recombination and trapping terms with trap concentrations N and actual charges ρ as well as the respective cross sections S, all as presented in Fig. 1. Of course, the current equation $j_{\mathrm{DHT}}^{\mathrm{DHR}}$ for holes (H) looks adequate.

The field direction factor F_{E} of generated electrons, initially moving in an electric field F, is explained by Monte Carlo calculations[19] and approximated with Eq. (2) for electrons and holes, respectively.

$$F_{\mathrm{H}}^{\mathrm{E}} = \frac{1}{2} \mp \frac{1}{2} \tanh \frac{F}{F_{\mathrm{H0}}^{\mathrm{E0}}} \quad (2)$$

The Poole–Frenkel release[24,25] of charges from traps is given by Eq. (3):

$$W_{\mathrm{HPF}}^{\mathrm{EPF}} = f_{\mathrm{H}}^{\mathrm{E}} \exp\left[-\frac{E_{\mathrm{H}}^{\mathrm{E}} - \Delta E_{\mathrm{PF}}}{kT} \right] \quad (3)$$

with the trap barrier lowering ΔE_{PF} due to an electric field F given in Eq. (4):

$$\Delta E_{\mathrm{PF}} = 2 \frac{e^{3/2}}{(4\pi\varepsilon_0\varepsilon_{\mathrm{r}})^{1/2}} F^{1/2} = \beta_{\mathrm{PF}} F^{1/2} \quad (4)$$

For the relevant dielectric and insulating materials alumina and silica we get the trap barrier lowering:

$$\frac{\Delta E_{\mathrm{PF}}}{eV} = 10^4 \left(\frac{e}{\pi\varepsilon_0\varepsilon_{\mathrm{r}}} \right)^{1/2} F_{\mathrm{MV/cm}}^{1/2} \simeq \begin{cases} 0.24\,\mathrm{eV} F_{\mathrm{MV/cm}}^{1/2} & \text{for } Al_2O_3; \quad \varepsilon_{\mathrm{r}} = 10 \\ 0.38\,\mathrm{eV} F_{\mathrm{MV/cm}}^{1/2} & \text{for } SiO_2; \quad \varepsilon_{\mathrm{r}} = 4 \end{cases} \quad (5)$$

We may describe the trapping and detrapping processes by first-order kinetics. Thus, an incident current density j leads to an actual trap occupation rate $n_T(t)$ with time t:

$$\mathrm{d}n_\mathrm{T} = +\frac{j}{e_0}(N - n_\mathrm{T})S\,\mathrm{d}t - n_\mathrm{T} f\,\exp\left(-\frac{E_\mathrm{T} - \Delta E_\mathrm{PF}}{kT}\right)\mathrm{d}t \tag{6}$$

where the second term means the Poole–Frenkel release of trapped charge (detrapping). N is the existing trap concentration, S the capture cross section, f an "attempt of escape frequency factor", shortly called pre-exponential "frequency factor", and ΔE_PF is the lowering of the thermal activation energy E_T by an electric field F, i.e. the Poole–Frenkel effect, as described by Eqs. (3) and (4).

In the following we have tested the trapping and Poole–Frenkel release mechanism by means of time-dependent filling and detrapping of the balance Eq. (6) and its iterative integration $t = t + \Delta t$. Thus, we get the partial filling rates as presented in Fig. 2.

From these calculation we may deduce an appropriate frequency factor dependence on the trap activation energy, see Fig. 3:

$$\log f = 4 + 5E_\mathrm{T}(\mathrm{eV}). \tag{7}$$

where f is given in s^{-1} and the activation energy E_T in eV.

Then the resulting charges will be counted from the balance of trapping and detrapping probabilities as well as from current fluctuations (divergences) as described detailled in ref.[23]

3. Samples with open and metal-covered surfaces

The problem of electron beam charge injection in different target arrangements is demonstrated in Fig. 4. Incident electrons (so-called primary electrons PE) with initial energy E_0 and current density j_0 penetrate the insulator target up to the maximum range $R(E_0)$ and create a mainly positive–negative spatial charge distribution $\varrho(x)$ where the positive charge beneath the surface is due to secondary electron (SE) escape into vacuum (open sample) or into an electrode upon the surface (coated sample). According to the electrode arrangements the charges will create different field and potential distributions $F(x)$ and $V(x)$, respectively, with a low surface field $F(x = 0) \simeq 0$ and a high floating surface potential V_0 for the open sample and a fixed zero surface potential for the grounded surface $V_0 = 0$, see Fig. 4(below). However, the latter one shows a high electric field beneath the surface.

The electric field $F(x, t)$ in open samples (Fig. 4, above) is calculated by successive summation (integration) of charges beginning from the surface into the bulk, i.e. towards the grounded support, see Fig. 4, because the sample support is the nearest electrode to the incorporated charges, usually much closer than any other metallic parts of a scanning electron microscope (SEM). Thus, the electric field of all charges possesses a component into the sample and the field at the surface $F(x = 0)$ is nearly zero.

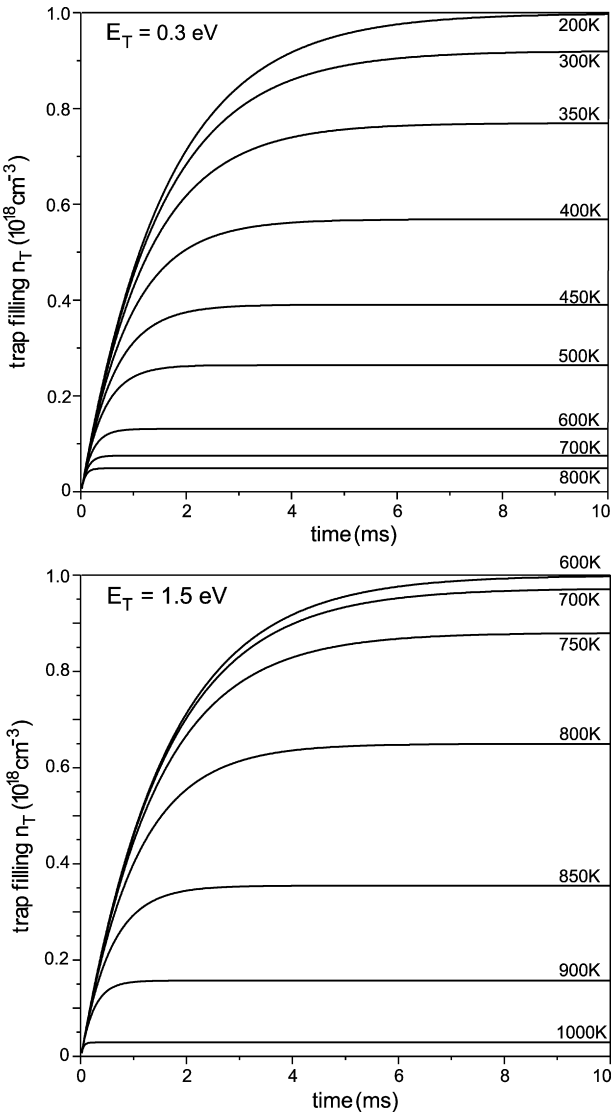

Fig. 2. Trapping and detrapping rates of charge carriers in localized states (traps) with concentration $N = 10^{18}\mathrm{cm}^{-3}$ and thermal activation energies $E_\mathrm{T} = 0.3$ and 1.5 eV, respectively, according to Eq. (6).

Of course, the metal-coated sample (Fig. 4, below) presents a special case of the previous procedure with the fixed value $V_{0,\mathrm{metal}} = 0$ and all field contributions of incorporated charges are directed to the close metallic surface electrode, vice versa, as for open samples where the field components are directed to the support (as the closest electrode). But here, in metal-coated samples, the electron penetration depth R of about 3 μm can be neglected with respect to the bulk sample thickness d of several millimeters.

4. Results and discussion

Open samples possess an open, non-covered surface and the secondary electron emission is only limited by the height of the surface barrier, i.e. by the electron affinity $\chi_{\mathrm{Al_2O_3}} = 0.9$ eV. Of course, all holes and also low energy drifting electrons will be totally reflected at the surface barrier. The total current

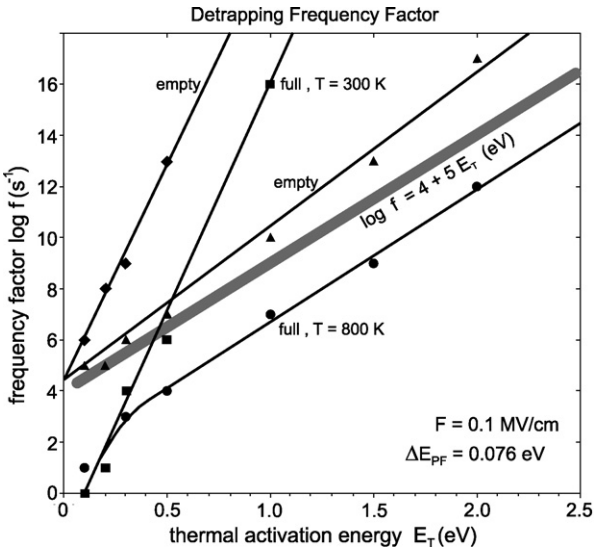

Fig. 3. Detrapping frequency factor f of charge release from traps with thermal activation energy E_T, demonstrating the range of full to empty traps for two temperatures $T = 300$ and 800 K according to Eq. (6) and Fig. 2.

$j_{tot}(x)$, the charge $\rho(x)$ and field $F(x)$ distributions in dependence on electron beam irradiation time $t = (10, \ldots, 100)$ ms ($E_0 = 20$ keV, $j_0 = 10^{-5}$ A/cm^2) are presented in Fig. 5(left). At the surface, we see the built-up of a positive charge distribution with a center of gravity at about 2.5 nm. The field is increasing positively enforcing field-enhanced secondary electron emission into the vacuum. The field remains positive up to 0.5 μm sweeping electrons towards the surface and holes into the bulk. Then, beyond 0.5 μm, the field changes to negative values and keeping almost constant up to the support electrode at $x = d = 3$ mm. The drifting and finally trapped charges form a four-fold charge distribution: plus–minus–plus–minus. The positive surface charge is due to emitted SE and remaining holes as we have obtained already by the former only ballistic model.[16]

Here we should mention, that all distributions, especially of $j_{tot}(x)$ and $\rho_{tot}(x)$ are shrinked towards the surface and do not reach the electron maximum range $R(E_0)$ in a remarkable extend. The reason for that is given by the overall negative charging and the resulting negative surface potential V_0. After 10 ms irradiation it approaches already −13 keV and the resulting initial energy of the incident electron beam is $E_0' = E_0 + eV_S = 7$ keV, see ref.[23]

As already mentioned in context with metal-covered samples and Fig. 4 thin metal or conducting material layers, like carbon, electrically grounded, are conventionally used to avoid surface charging of insulating samples. These layers are mostly evaporated or sputtered onto the surface, their thickness is very thin, about 10 nm, in order not to affect the incident electron beam so much.

As we see in Fig. 5(right) the distributions of currents, charges, fields and potentials are shown for surface potential-fixed layers $V_0 = 0$. They show much less fluctuations than for open layers in Fig. 5(left). The plus and minus charges are located near to the surface and the field is thoroughly positive increasing towards the surface up to 0.3 MV/cm. The negative potential shows a maximum of only −27 V in the depth, nearly at the maximum range $R \approx 3$ μ m of the incident electrons with energy $E_0 = 20$ keV. Thus, the incident and spatially exciting electron beam is not affected by retarding field effects. Thus, the main intention of charging prevention is fulfilled, however, the greatest affect to the SEE measurements, spectroscopy or microscopy is given by the electron scattering in the metallic or conducting material layer on the surface. Therefore, preference should be given to positive-ion-covered surfaces as discussed also in ref.[23] in context with ESEM, or even to charge neutralization by "low energy electron rinsing" as commonly used in electron spectroscopy of insulating samples.

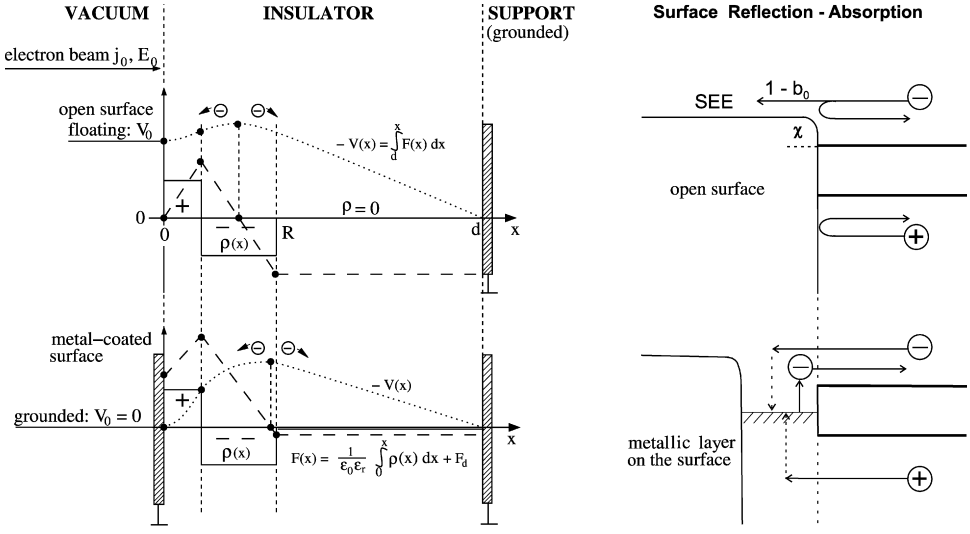

Fig. 4. Plus–minus charge distribution $\rho(x)$ beneath the surface and the respective electrical field $F(x)$ and potential $V(x)$ distributions in a dielectric sample on conducting support with an open surface (above) and a metal covered and grounded surface (below). On the right, the reflection and/or absorption of electrons and holes at the respective surfaces are shown.

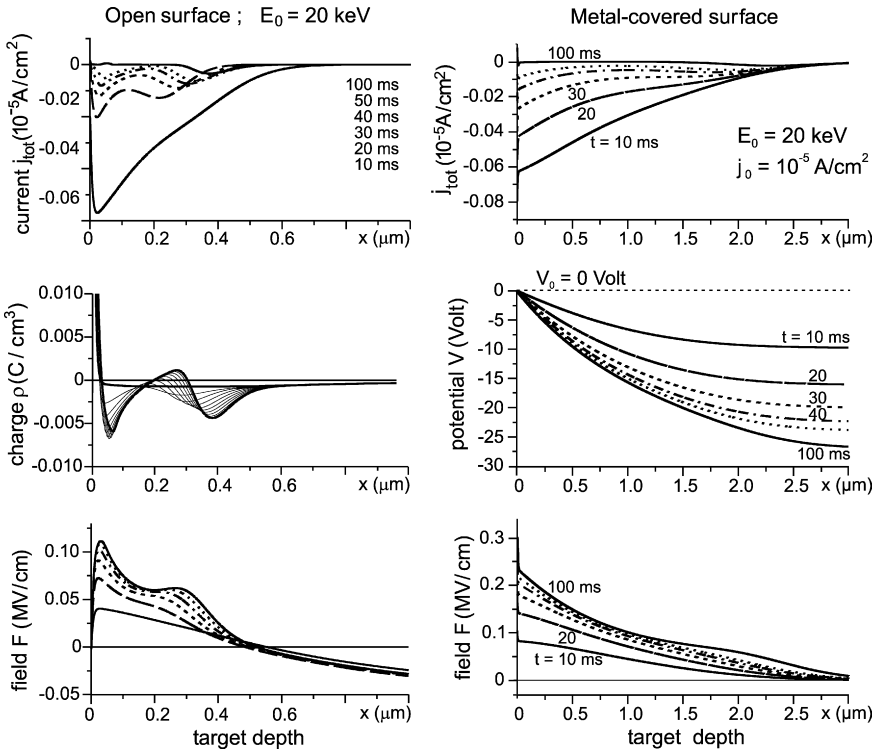

Fig. 5. Total current $j_{tot}(x)$, charge $\rho(x)$, and field $F(x)$ depth distributions in a bulk (3 mm) Al_2O_3sample as a function of irradiation time t for an initial beam energy of $E_0 = 20$ keV and current density $j_0 = 10^{-5}$A/cm^2; left: in an open surface sample; mention that all the bulk distributions are shrinked towards the surface because of a strong negative charging and respective retarding of the electron beam to $E_0' = E_0 - eV_0 = 7$ keV; contrary to right: for a metal-covered and grounded surface ($V_0 = 0$).

5. Conclusions

The new flight-drift model of selfconsistent electron transport and electrical charge storage in wide-gap insulators reflects a more realistic simulation of these processes in dielectric and insulating materials. Electron-hole creation, their ballistic flight, followed by field-drift transport, and finally trapping in localized states and/or recombination are taken into account. The experimentally accessable quantities of field assisted secondary electron emission σ as well as the resulting surface potential V_0 due to internal current $j(x, t)$, charge $\rho(x, t)$, field $F(x, t)$, and potential $V(x, t)$ distributions are obtained.

The charging of open, i.e. non-covered and floating insulating bulk samples is strongly controlled by the surface potential $V_0(x = 0)$ and the consequent electron beam retarding for negative charging $V_0 < 0$ or even beam accelleration for positive charging $V_0 > 0$ according to the affection of the initial energy $E_0' = E_0 + eV_0$. Thus, the maximum range of incident primary electrons is rapidly diminished for high beam energies $E_0 > 5$ keV by negative charging and the internal current, charge and field distributions are shrinked strongly towards the surface.

A similar effect is given in conventional metal or conducting material coated insulating samples. Usually the coating layer is grounded and no electron beam retarding field effects are observed, also within the sample where the negative potential distribution does not exceed several tens of Volt, i.e. $V(x) < -50$ V. Thus, the exciting electron beam is not affected neither in the front of the surface in vacuum nor in the internal bulk insulator. However, one cannot neglect the additional scattering of the incident electron beam as well as of backscattered and secondary electrons within the coating layer. Thus, in order to prevent charging, the positive-ion-covered surface bears certain advantages versus metal coating.

References

[1]. Mannhart, J. and Schlom, D. G., *Physik Journal*, 2005, **4**(June (6)), 45–51.
[2]. In *4th International Conference on Electric Charges in Non-Conductive Materials Vol. Special CSC'4*. Science, Techniques et Applications, Le Vide, 2001.
[3]. Gauvin, R., ed. *Symposium on Characterization of Non-Conductive and Charging Materials by Microbeam Analysis*. McGill University Montreal, Canada, August 2002.
[4]. Ibarra, A. and Hodgson, E. R., The ITER project: the role of insulators. *Nucl. Instrum. Methods Phys. Res. B*, 2004, **218**, 29–35.
[5]. Griseri, V., Fukunaga, K., Maeno, T., Levy, L., Laurent, C. and Payan, D., *IEEE Trans. Dielectr. Electr. Insul.*, 2005, **11**, 891–898.
[6]. Levy, L., Material Charging, Cedapus Editions 2002, pp. 241–266.
[7]. Melchinger, A. and Hofmann, S., *J. Appl. Phys.*, 1995, **78**, 6224–6232.
[8]. Cazaux, J., *J. Appl. Phys.*, 1999, **85**, 1137–1147.
[9]. Vicario, E., Rosenberg, N. and Renoud, R., *Surf. Interface Anal.*, 1994, **22**, 115–119.
[10]. Ganachaud, J. P., Attard, C. and Renoud, R., *Phys. Status Solidi (b)*, 1997, **199**, 175–184 and 455–465.
[11]. Renoud, R., Mady, F. and Ganachaud, J. P., *J. Phys.: Condens. Matter*, 2002, **14**, 231–247.
[12]. Mady, F., Renoud, R., Attard, C., Bigarré, J., Ganachaud, J.-P. and Hourquebie, P., *Eur. Phys. J. Appl. Phys.*, 2002, **20**, 41–53.
[13]. Fitting, H.-J., Habilitation Thesis, University of Rostock, Germany, 1978.

[14]. Fitting, H.-J., Glaefeke, H., Wild, W., Franke, M. and Müller, W., *Exp. Tech. Phys. (Berlin)*, 1979, **27**, 13–24.
[15]. Glavatskikh, I. A., Kortov, V. S. and Fitting, H.-J., *J. Appl. Phys.*, 2001, **89**, 440–448.
[16]. Meyza, X., Goeuriot, D., Guerret-Piécourt, C., Tréheux, D. and Fitting, H.-J., *J. Appl. Phys.*, 2003, **94**, 5384–5392.
[17]. Fitting, H.-J., Glaefeke, H., Wild, W. and Ulbricht, R., *Exp. Tech. Phys. (Berlin)*, 1976, **24**, 447–458.
[18]. Hingst, Th., Hübner, M., Franz, R., Kuhr, Ch. and Fitting, H.-J., *Microelectr. Eng.*, 1994, **24**, 181–188.
[19]. Fitting, H.-J. and Friemann, J.-U., *Phys. Status Solidi (a)*, 1982, **69**, 349–358.
[20]. Fitting, H.-J. and Boyde, J., *Phys. Status Solidi (a)*, 1983, **75**, 137–142.
[21]. Schreiber, E. and Fitting, H.-J., *J. Electron Spectrosc. Relat. Phenom.*, 2002, **124**, 25–37.
[22]. Fitting, H.-J., Schreiber, E. and Glavatskikh, I. A., *Microsc. Microanal. (U.S.A.)*, 2004, **10**, 764–770.
[23]. Touzin, M., Goeuriot, D., Guerret-Piécourt, C., Juve, D., Tréheux, D. and Fitting, H.-J., *J. Appl. Phys.*, 2006, **99**, 114110-1-14.
[24]. Frenkel, J., *Phys. Rev.*, 1938, **54**, 647–648.
[25]. O'Dwyer, J. J., *The Theory of Electrical Conduction and Breakdown in Solid Dielectrics*. Clarendon Press, Oxford, 1973.